Prediction model for the initial seed clearing angles of a precision seed meter based on vector fields

Wan Jiao[1], Junjie Zhang[1], Xuhui Chen[1], Hao Shen[1], Yuxiang Huang[1*], Jiangtao Shi[2]
(1. *College of Mechanical and Electric Engineering, Northwest A & F University, Yangling 712100, Shaanxi, China*;
2. *Xi'an YaAo Agricultural Machinery Ltd, Xi'an 710300, China*)

Abstract: Seed clearing is a critical stage during precision seed metering process to ensure high seed singulation. However, there is a lack of understanding of the dynamics in the seed clearing process. In this study, a model was developed to predict initial seed clearing angle, in the seed clearing process using vector fields. The model was applied to an existing high-speed metering device and soybean seeds, and the model was evaluated with bench testing results. Results showed that dynamic changes in forces and constraints of seeds during the seed clearing process could be abstracted as vectors, and the changes of vector directions could be described by their phase angles. The phase angles were functions of the rotational angle of the seed meter. The phase angle of the constraint boundary linearly increases with the increase of the rotational angle. The phase angle of the force fluctuates, as the rotational angle changes. Initial seed clearing angle obtained from the phase angles varies from 8° to 59°, depending on the seeder travel speed. When comparing the values of the initial seed clearing angles predicted by the model with those from the bench tests, the root mean square error (RMSE) were from 2.73 to 3.14, and the correlation (r) between predict and observer were all higher than 0.98, indicating that the model had reasonably good accuracy.

Keywords: mechanical precision seeder, initial seed clearing angle, prediction model, vector fields, high-speed photography technology
DOI: 10.25165/j.ijabe.20241702.7029

Citation: Jiao W, Zhang J J, Chen X H, Shen H, Huang Y X, Shi J T. Prediction model for the initial seed clearing angles of a precision seed meter based on vector fields. Int J Agric & Biol Eng, 2024; 17(2): 140–148.

1 Introduction

High-speed precision seeding has become the direction of modern seeding technology because of its cost-effective and high-efficiency advantages over other seeding technologies, such as drilling and broadcasting. Precision seed meter is the core component of a precision seeder[1,2]. Precision seed meters can be classified into two major types: vacuum-type and mechanical-type. Compared with vacuum-types, mechanical-types are simpler in structure and more cost effective[3,4]. In some areas with scattered plots and small area, and the surrounding non cultivated land can not be planted uniformly, mechanical seed meter is still widely used. For example, mechanical seed meter has been widely used in soybean and corn planting areas in China[5].

The working process of a mechanical precision seed meter can be generally divided into four stages: filling, clearing, carrying, and dropping of seeds[6-8]. During the filling stage, seeds are filled into the seed-cells of the meter. In the clearing stage, surplus seeds in the seed-cell are cleared out so that only one seed remains in the cell; this process is referred to as singulation[9]. The singulated seed is carried over to the next stage, and eventually dropped into the soil. Existing mechanical seed meters do not have an efficient and effective seed clearing process due to the lack of understanding of the dynamic interaction between the seeds and the meter.

There are several design and operational parameters which affect the clearing performance of a mechanical precision meter. Among them, initial clearing angle is the critical one. Initial seed clearing angle is defined as the angle between the seed and the horizontal plane when the seed is departing from the seed-cell of the seed meter. It represents the beginning of the clearing process, and it significantly affects the effectiveness of the clearing. In recent years, research was carried out on the seed clearing process of precision seed meters. Forces on the seeds and their corresponding motions during the clearing process have been studied under different geometries and operational parameters of different seed metering devices. A kinematic equation describing the motion of seeds to be cleared in relation to the motion of the metering disc was established, and a conclusion was drawn that the initial clearing angle increases with the increase of the rotational speed of the metering disc[10]. Based on the static equilibrium of forces, a relationship was established between the initial clearing angle and the rotational speed, vertical inclination angle, and the diameter of the meter disc[11]. With the equilibrium of the radial forces on seeds, the trend of changes in the seed initial clearing angle was obtained under different working conditions of a soybean seed meter[12]. In these existing studies, constantly changing forces and directions of the seeds while the metering disc rotates have not been well documented. Therefore, it is very important to predict the initial seed clearing angle for further studying the working mechanism of the mechanical precision meter, providing a theoretical basis for the design of the mechanical precision seed meter.

The objectives of this study are as follows: (1) Developing a model based on vector fields to predict initial seed clearing angles.

Received date: 2021-08-26 **Accepted date:** 2023-12-27
Biographies: **Wan Jiao**, Undergraduate, research interest: agricultural engineering, Email: 365288003@qq.com; **Junjie Zhang**, PhD candidate, research interest: agricultural engineering, Email: 1285770127@qq.com; **Xuhui Chen**, MS candidate, research interest: agricultural engineering, Email: 2021051006@nwafu.edu.cn; **Hao Shen**, MS candidate, research interest: agricultural engineering, Email: 290605237@qq.com; **Jiangtao Shi**, Engineer, research interest: agricultural mechanization and automation.
***Corresponding author: Yuxiang Huang**, PhD, Professor, research interest: agricultural engineering. Northwest A&F University, Yangling 712100, Shaanxi, China; Tel: +86-29-87092391, Email: hyx@nwsuaf.edu.cn.

(2) Evaluating the accuracy of the prediction model by applying the prediction model to the double-holding precision seed meter and soybean seeds.

2 Methodology

2.1 Development of prediction model

A prediction model was developed to predict initial seed clearing angles based on analyses of dynamic interactions between seeds and the metering device. The model development included analyses of the constraints and forces that the seeds are subjected to during the clearing stage of the metering process. Such analysis involved multiple constraint reaction forces and external forces. Based on the theory that the reaction force acting on a particle does not change its existing trajectory, all constraint reaction forces to the seed were abstracted as one restraint vector, and all external forces were superposed as an external force vector. Phase angle functions of these vectors were established, and they were utilized to predict the initial seed clearing angle in the precision metering process.

2.1.1 Analysis of the constraint boundary vector

Constraint reaction forces acting on seeds come from the precision metering device, and they vary depending on the type of metering device. There is a typical type of precision seed metering disc: a double-holding seed-cell (Figure 1)[13]. In the seed clearing process, there could be multiple seeds in the seed-cell. An example of having two seeds in the seed-cell is shown in Figure 1. These two seeds are referred to as Seed No.1 and Seed No.2. Seed No.2 is to be cleared out of the seed-cell, while Seed No.1 is to be carried to the next stage. Thus, the relevant seed in the following discussion is referred to as Seed No.2. The coordinate origin is positioned at the center of Seed No.2. The constraints to the seed are described by several parameters in the *X*-*Z* plane. The range of the constraint that the seed was subjected to is expressed by an angle of A, namely the constraint angle, which is formed by α_1 and α_2, named as constraint boundaries. These parameters vary with the geometry of the seed-cell. For example, the constraint angle (A) of the spoon-type seed-cell has a different position in the *X*-*Z* plane as compared with the other two types of seed-cell. Regardless, within A, Seed No.2 is always restricted and does not have any motion.

In developing the prediction model, a complex plane with a real axis (Re-axis) and an imaginary axis (Im-axis) was established on the plane of seed metering disc (Figure 2a). The origin of the complex plane coincides with the center of the metering disc. The variation of seed shape and size affects the centroid of both Seeds No.1 and No.2, and the origin of the *X*-*Z* coordinates. This variation in subspherical seeds can be described by a deviation angle (α) between the centroid line and the *X*-axis (Figure 2b).

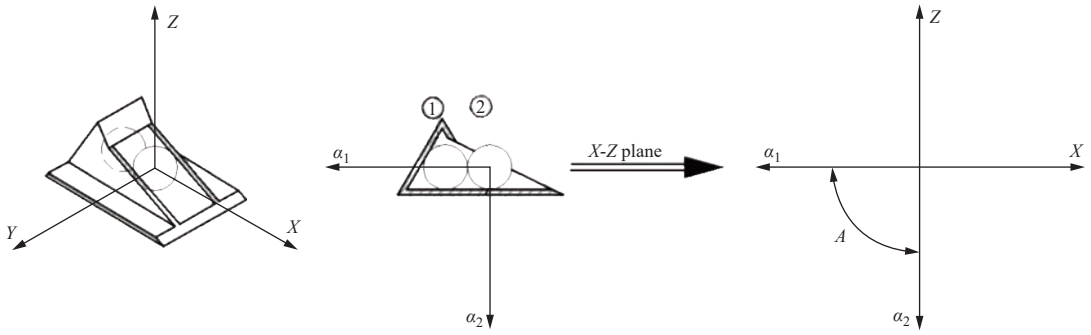

Figure 1 Constraint angles (A) formed by the constraint boundaries of α_1 and α_2

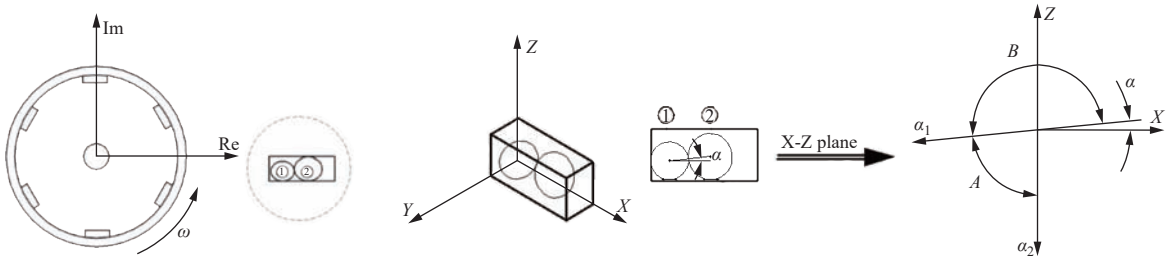

Note: ω is angular velocity of the disc, rad/s.
a. The complex plane on metering disc

b. An enlarged seed-cell with Seeds No.1 and No.2, deviation angle (α), constraint angle (A) formed by the constraint boundaries of α_1 and α_2, angle (B) is 180°

Note: ω is angular velocity of the disc, rad/s.

Figure 2 The constraint boundary vector of seed metering disc and seed cell

The α affects the magnitude of the angles, A and B. The deviation angle is calculated by:

$$\alpha = \tan^{-1}\left(\frac{L_{z2}-L_{z1}}{L_{x2}+L_{x1}}\right) \quad (1)$$

where, α is the deviation angle, (°); L_{z1} and L_{z2} are the dimensions (mm) in *Z*-axis of Seeds No.1 and No.2, respectively; L_{x1} and L_{x2} are the dimensions (mm) in *X*-axis of Seeds No.1 and No.2, respectively.

While the metering disc rotates counterclockwise at an angular velocity of ω (Figure 2a), the seed-cell rotates as well. As a result, the direction of the constraint boundary vector (α_1 and α_2) changes (Figure 2b). To describe the change as a function of the rotational angle (θ) of the meter disc, a complex function, $f_c(\Delta\theta)$, was used to represent the counterclockwise rotating direction of the constraint boundary vector. The representative of the positive direction of *X*-axis direction is the positive Re-axis of complex function, the positive Im-axis of complex function is on behalf of the *Z*-axis, in this way, $f_c(\Delta\theta)$ is expressed as:

$$f_c(\Delta\theta) = \boldsymbol{a}[\cos(\Delta\theta+\alpha+B)+i\sin(\Delta\theta+\alpha+B)] \quad (2)$$

where, a is the unit vector, (°); θ is the rotation angle (counterclockwise) of the seed metering disc, (°); $\Delta\theta$ is the angle increment of θ, (°); i is the positive direction vector of the Im-axis.

2.1.2 Analysis of the external force vector

The seed is subjected to various external forces, including

centrifugal force, gravitational force, and frictional force. These forces were abstracted as an external force vector through the superposition of three vector fields. The vector fields were expressed on the complex plane built on the seed metering disc as shown in Figure 2a. As the seed in the seed-cell rotates with the metering disc, the seed follows a circular trajectory. Thus, the external force vectors act on the circular trajectory and vary with the θ of the metering disc, as discussed below.

The direction of the centrifugal force is the function of the θ in the complex plane as:

$$\boldsymbol{a}_c = \cos\theta + i\sin\theta \tag{3}$$

where, $\boldsymbol{a}_c$ is the direction of centrifugal force. The centrifugal force is determined by the mass of seed, and the radius and angular velocity of the seed metering disc as follows:

$$F_c = \omega^2 Rm \tag{4}$$

where, m is the mass of seed, kg; R is the rotating radius of the seed metering disc, m.

The complex function describing the centrifugal force field is equal to the product of the direction (Equation 3) and magnitude (Equation 4) of the centrifugal force as:

$$F_c(\theta) = \omega^2 Rm(\cos\theta + i\sin\theta) \tag{5}$$

The centrifugal force acting on the seed is linearly related to the θ. The direction of the centrifugal force is radially outwards in the complex plane (Figure 3a). In contrast, the direction of the gravitational force of seed does not change with the θ (Figure 3b). The complex function of gravity field is as follows:

$$F_G(\theta) = -mgi \tag{6}$$

where, g is the gravity acceleration, m/s^2. The negative sign in Equation 6 indicates that the gravity direction is opposite to the positive direction of the Im-axis.

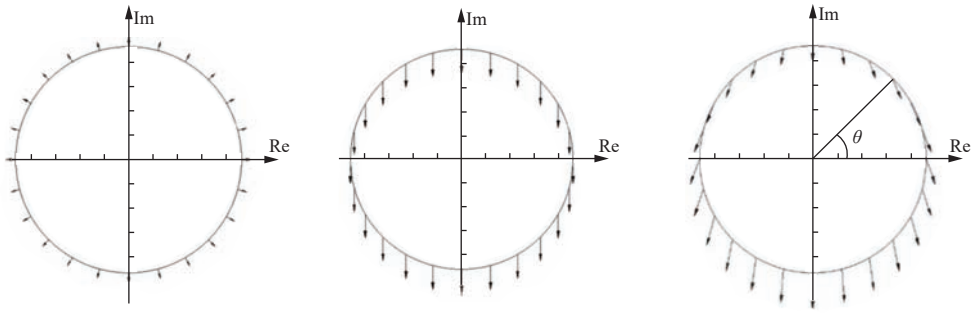

a. Centrifugal force field b. Gravitational force field c. Force vectors of the superposition field of the two force fields.

Figure 3 Vector fields of the seed in complex plane

Frictional forces occur at the contacts between the seed and neighboring seeds and between the seed and seed-cell walls. The direction of frictional force depends on the direction of seeds departing from the contact surface. The complex function of frictional force is determined by the specifications of the seeds and seed-cell geometries, but it can be expressed as the following general form:

$$F_f(\theta) = F_{Re}(\theta) + F_{Im}(\theta) \tag{7}$$

where, F_f is the unit friction (N); F_{Re} and F_{Im} are the components of the frictional forces which are parallel to the Re-axis and Im-axis respectively.

Given the aforementioned three force fields: centrifugal, gravity, and friction fields, the field of the external force vector can be obtained by their superposition as follows:

$$f_f(\theta) = \omega^2 Rm(\cos\theta + i\sin\theta) - mgi + F_{Re}(\theta) + F_{Im}(\theta) \tag{8}$$

where, $f_f(\theta)$ is the force vector function of superposition field. The superposition field is illustrated in Figure 3c. Both the direction and magnitude of the superposition field varied with θ.

2.1.3 Phase angle functions

The relationship between the external force vector and constraint boundary vector was described using phase angles (ϕ) established in the θ–ϕ coordinate system, where ϕ is the dependent variable and θ is the independent variable. Phase angle is obtained by rotating counterclockwise from the positive Re-axis, and it ranges from 0 to 360°. The general expression of phase angle is:

$$\phi = \arctan\frac{I_m}{R_e} \tag{9}$$

where, ϕ is the phase angle, (°). The change in constraint angle is as following equation:

$$\Delta\theta = \theta - \theta_0 \tag{10}$$

where, θ_0 and $\Delta\theta$ is the initial constraint angle and increment (°), respectively.

By replacing the $\Delta\theta$ in Equation (2) by $\theta - \theta_0$, one obtains the constraint boundary vector as:

$$f_c(\theta) = a[\cos(\theta + \alpha - \theta_0 + B) + i\sin(\theta + \alpha - \theta_0 + B)] \tag{11}$$

where, θ_0 is the initial disc rotational angle, (°). From Equations (9) and (11), the phase angle function for the constraint boundary vector is obtained as follows:

$$\phi_c(\theta) = \arctan\frac{\sin(\theta + \alpha - \theta_0 + B)}{\cos(\theta + \alpha - \theta_0 + B)} \tag{12}$$

where, ϕ_c is the phase angle of the constraint boundary vector.

The above equation was further simplified as:

$$\phi_c(\theta) = \theta + \alpha - \theta_0 + B \tag{13}$$

The phase angle function of force was obtained from the imaginary and real components of the superposition field function according to Equations (7) and (8):

$$[f_f(\theta)]_{Im} = \left(-mg + \omega^2 Rm\sin\theta\right) i + F_{Im} \tag{14}$$

$$[f_f(\theta)]_{Re} = \omega^2 Rm\cos\theta + F_{Re} \tag{15}$$

where, $[f_f(\theta)]_{Im}$ and $[f_f(\theta)]_{Re}$ are the Im-axis and *Re*-axis components of the superposition filed respectively. By substituting Equations (14) and (15) into Equation (9), the phase angle function

of the external force vector is obtained as:

$$\phi_f(\theta) = \arctan\frac{-mg+\omega^2 Rm\sin\theta + f_{Im}}{\omega^2 Rm\cos\theta + f_{Re}} \quad (16)$$

where, ϕ_f is the phase angle of the external force vector.

2.1.4 Prediction of initial seed clearing angle

Equations 13 and 16 describe the dynamics of the constraint reactions and external forces acting on the seed. The equations were solved with input parameters, including the initial position of the seed-cell, the rotational speed of the metering disc, and the dimensions of the seeds. Response surface methodology[14] was used to examine the phase angle functions of ($\phi_c(\theta)$) and ($\phi_f(\theta)$) under various rotational angles (θ) of the metering device. The vector α_1 is the initial constraint boundary vector. Once the external force vector acting on the seed crosses this initial constraint vector, the seed clearing stage commences. Thus, the intersection points of the two surfaces are considered to be the initial seed clearing angles. As shown in Figure 4, when the metering disc rotates counter-clockwise, the position relationship between the external force vector and the constraint boundary vector changes constantly. Coincidence of the external force vector and the constraint boundary vector was the beginning of clearing.

2.2 Case study of using the prediction model

2.2.1 Description of the seeds and seed metering device

The variety of the soybean seeds used in the case study was SuiNong 26 (1000-kernel weight: 231.02 g). As shown in Figure 5, the shape of the soybean seed was quantified by the triaxial dimensions: length (L), width (W), and thickness (T)[15]. A total of 200 soybeans were selected, and their triaxial dimensions were measured using a vernier caliper with an accuracy of 0.01 mm.

The metering device used in the case study was a high-speed mechanical precision meter developed by Xue et al.[13] The metering device had a double-holding seed-cell (Figure 6a). The diameter of the metering disc was 220 mm. Travel speed significantly affected the performance of a precision seeder[16,17]. In the case study, various travel speeds (8, 9, 10, 11, and 12 km/h) of the seeder were considered[18].

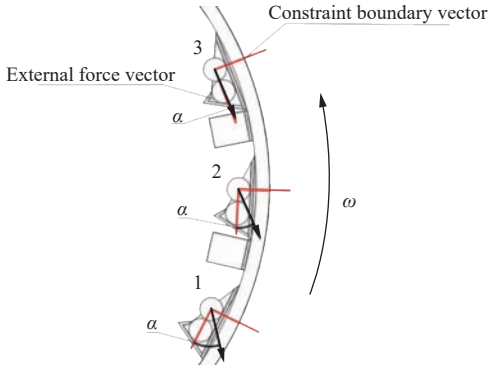

Figure 4 The change of external force vector and constraint boundary vector on clearing

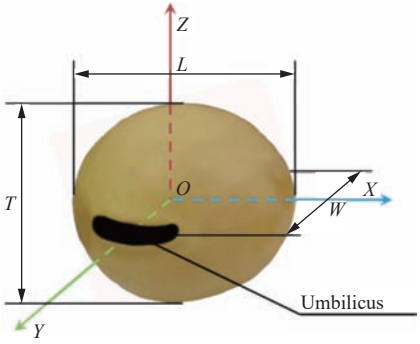

Figure 5 Triaxial dimensions and coordinate system of soybean seed

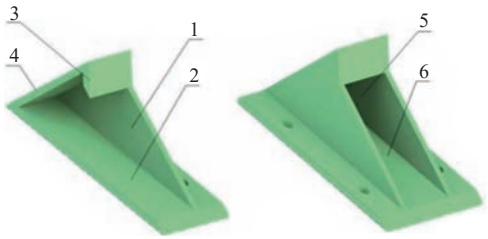

1.Side plate 2.Bottom plate 3.First holding plate 4.Second holding plate 5.Seed-cell 6.Guiding groove

a. Double-holding seed-cell

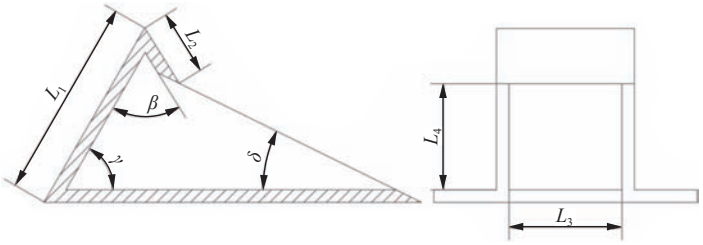

L_1 and L_2 are the lengths of the first and second holding plates; L_3 and L_4 are the picker opening dimensions; γ is the seed cell angle; β is the seed holder angle; δ is the side plate angle.

b. Dimension of the double-holding seed-cell

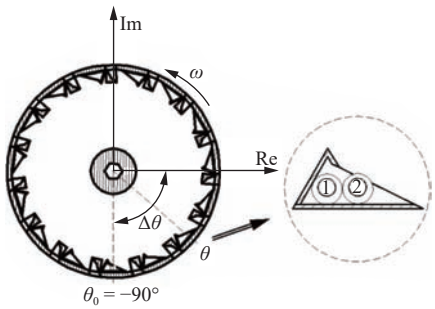

c. The metering disc, complex plane, and initial position for analyses

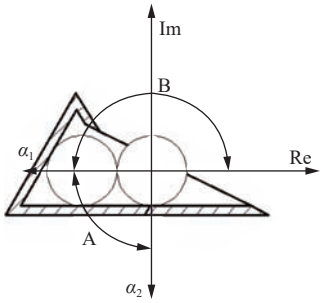

d. Constraint angle (A), constraint boundaries (α_1 and α_2), and angle (B) between constraint angle and Re-axis

1. Side plate 2. Bottom plate 3. First holding plate 4. Second holding plate 5. Seed-cell 6. Guiding groove L_1 and L_2 are the lengths of the first and second holding plates; L_3 and L_4 are the picker opening dimensions; γ is the seed cell angle; β is the seed holder angle; δ is the side plate angle.

Figure 6 The metering device used in the case study

2.2.2 Initial conditions for the model

The Initial position of the seed cell is set at –90° (Figure 6b). The position of the seed cell in the vector field is [–90°, 270°]. The boundaries (α_1 and α_2) of the constraint angle A and angle B are shown in Figure 6c.

2.2.3 Phase angle functions for the case study

The phase angle function of the constraint boundary vector ($\phi_c(\theta)$) in the case study was the same as Equation 13. As for the phase angle of the external force vector ($\phi_f(\theta)$), the force analyses are shown in Figure 7. The centrifugal force field and gravitational field were similar to the aforementioned discussion. Here the frictional force field was analyzed using the specific geometric parameters of the double-holding seed-cell used in the case study. The frictional force acting on the seed is linearly related to the rotation angle (θ) of the seed meter. In order to ensure the sowing quality, the seed meter is usually filled with more than one seed. Therefore, the friction of the seed to be cleaned during the seed cleaning process is uniformly expressed by the parameter N due to the uncertainty of the seed filling quantity, which can be expressed in the complex plane as follows:

$$F_f = mg\cos\theta(\cos\theta+i\sin\theta) \quad (17)$$

where, μ is the rolling friction coefficient[13] and N is the correction coefficient. In practice, there could be a random number of seeds being filled in the seed-cell, due to the variation in seed size and shape[19]. This would result in a random change in the number of contacts between Seed No.2 and the surrounding seeds, leading to random changes in the frictional force of Seed No.2. Thus, a seed correction coefficient (N) was introduced, which is defined as the number of seeds to be cleared. If, on average, there are M seeds being filled in the seed-cell, N would be M-1, given the fact that one seed is kept in the seed-cell. Through a filling test using high-speed photography, the number of seeds filled in the seed-cell was observed under the rotating speed (8 km/h, 9 km/h, 10 km/h, 11 km/h, 12 km/h). 200 groups of data were recorded in each group. It was found that the number of seeds in the seed-cell increased with the increase of rotating speed. The number of N in the metering device increased gradually from 3 seeds at a lower rotation speed to 4 seeds at a higher rotation speed, in order to simplify calculation, an average value of N = 2.5 was observed and this value was used in the model calculations.

The force vector of superposition field can be obtained by Equations (5), (6) and (17) as:

$$F_f(\theta) = -mgi+\omega^2Rm(\cos\theta+i\sin\theta)+N\mu mg\cos\theta(\cos\theta+i\sin\theta) \quad (18)$$

The phase angle function of the external force vector in the superposition field is obtained from the Equations (9) and (18) as following:

$$\phi_f(\theta) = \arctan\frac{-mg+\omega^2Rm\sin\theta+N\mu mg\cos\theta\sin\theta}{\omega^2Rm\cos\theta+N\mu mg\cos^2\theta} \quad (19)$$

With the input parameters of the seed cell in the double-holding precision seed meters and the soybean seeds used, the phase angle functions ($\phi_c(\theta)$) and ($\phi_f(\theta)$) were solved using Matlab.

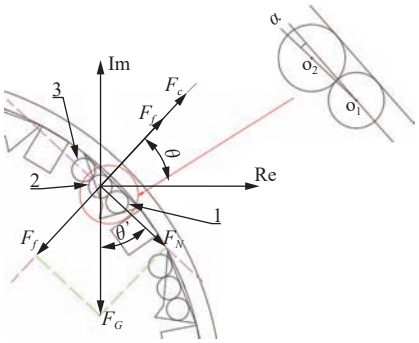

F_c, F_G, and F_f are centrifugal, gravitational, and frictional forces, respectively; θ is the rotational angle of the metering disc, θ' is equal to θ.

Figure 7 Analysis of the external forces of the soybean seed in the double-holding seed-cell used in the case study

2.3 Bench tests

2.3.1 Description of seeds and testing apparatus

Bench tests were carried out in May 2019 in the Seed Metering Laboratory, Northwest University of Agriculture and Forestry Science and Technology to measure the initial seed clearing angles. The measurements were used to evaluate the model predictions. The seeds used in the benching tests were soybeans (variety: SuiNong 26). The average dimension of the seeds was 7.53 mm in length, 7.14 mm in width, and 6.62 mm in thickness. The 1000 kernel weight was 231.0 g. The mechanical double-holding high-speed precision metering device described above was used for the tests.

2.3.2 Test procedure

The double-holding precision metering device was installed on a metal bench (Figure 8a). The metering device was driven by a motor (86HBP115AL4S-TK0, Times Brilliant Company, China) with a speed control (1-2000 r/min). During the test, the metering disc was covered with a transparent acrylic plate, so as to capture the dynamics of the seeds by a high-speed camera (SPEED TR, Olympus Company, Japan). The camera (750 fps) was controlled by a controller. The lens center of the camera was positioned in line with the shaft of the metering disc. The horizontal distance between the camera lens and the metering disc was 600 mm.

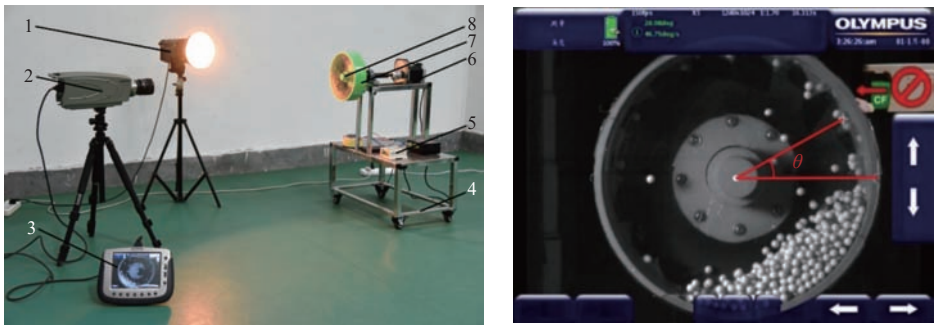

a. Bench testing apparatus b. An image from the camera controller interface

1. Lamp 2. high-speed camera 3. Camera controller 4. Test bench 5. Motor speed control system 6. Motor 7. Metering disc 8. Disc shaft

Figure 8 Testing system

During the tests, the motor speed was adjusted according to the preset rotational speeds of the metering disc. In each test run, the process of metering the soybean seeds was recorded by the camera for 80 s, and the video of the stable operation (from 5 to 80 s) was used for analysis. In the analysis, the centre of the metering disc was taken as the coordinate origin, and the horizontal line was used as the reference point (Figure 8b) to determine the initial clearing angle of soybean seeds. This measurement was done for each of the disc angular velocities of 4.65, 5.23, 5.80, 6.40, and 6.98 rad/s, corresponding to seeder travel speeds of 8, 9, 10, 11, and 12 km/h, respectively. Data points of outliers were deleted before analyses[20].

2.3.3 Validation of the prediction model

To evaluate the accuracy of the model, model predictions of initial seed clearing angles and the bench test results were compared. The agreement was assessed with the root mean square error (RMSE) and the correlation (r). The RMSE and r were calculated as:

$$\mathrm{RMSE} = \sqrt{\frac{1}{n}\sum_{t=1}^{n}\left(y_{\mathrm{observed}} - y_{\mathrm{predicted}}\right)^2} \tag{20}$$

$$r = \frac{Cov(y_{\mathrm{observed}}, y_{\mathrm{predicted}})}{\sqrt{D(y_{\mathrm{observed}})}\cdot\sqrt{D\left(y_{\mathrm{predicted}}\right)}} \tag{21}$$

where, y_{observed} is the value of bench test; $y_{\mathrm{predicted}}$ is value of model prediction; N is the number of tests; $Cov(\cdot)$ is covariance; $D(\cdot)$ is variance.

3 Results and discussion

3.1 Distribution of soybean seed dimensions

All triaxial dimensions of the soybean seeds followed a normal distribution (Figure 9). The length of seed varied the most, from 6.0 to 9.0 mm, and most seeds had a length between 7.1 and 7.7 mm. The majority (over 65%) of the seeds had a width of approximately 6.6 mm and a thickness of approximately 7.3 mm.

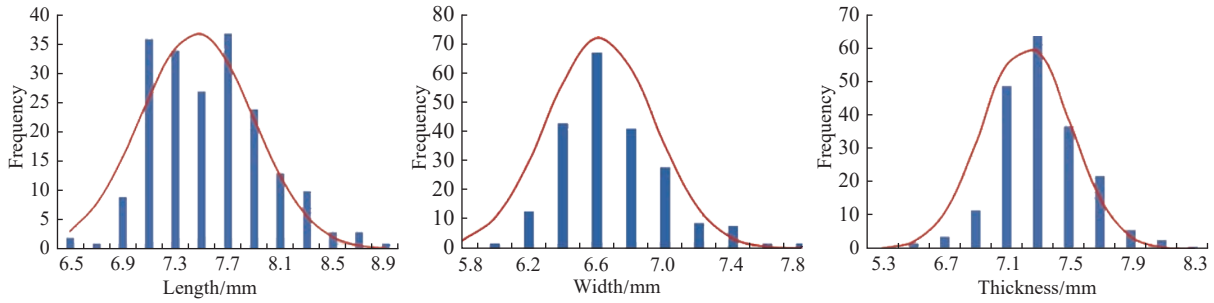

Figure 9 Distribution of the triaxial dimensions of 200 soybean seeds

3.2 Deviation angle of the soybean seeds

With 200 soybean seed samples and each seed having three dimensions, a total of 600 data points was obtained. These data points were imported into MATLAB to calculate the deviation angles (α) defined in Figure 2 using Equation 1. Results were plotted as a probability density curve (Figure 10). The probability density curve showed that the deviation angle of the soybean seeds varied from –8.2° to 8.2°, following a normal distribution.

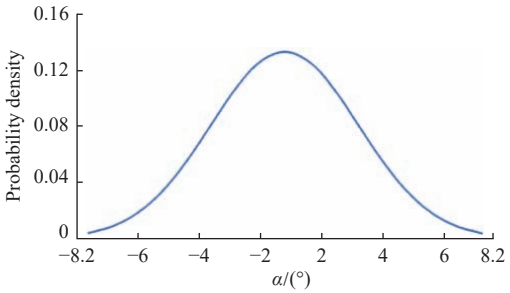

Figure 10 Distribution of deviation angle (α) of the soybean seeds

3.3 Phase angles of the constraint boundary vector

The model results of the phase angle of the double-holding precision metering device were plotted as a response surface across the disc rotational angle (θ) of –90° to 270° and the deviation angle (α) from –8.2° to 8.2° (Figure 11). At a constant α, the phase angle increases linearly with the θ; at a given θ, the phase angle increases slightly with the α.

3.4 Phase angle of the external force vector

The model input parameters used for the case study are listed in Table 1. With these input parameters, the model equation was solved by MATLAB to obtain the phase angles of the external force vector in the superposition field over ranges of α and θ values. The disc rotational speeds used correspond to the seeder travel speeds: 8, 9, 10, 11, and 12 km/h, as aforementioned.

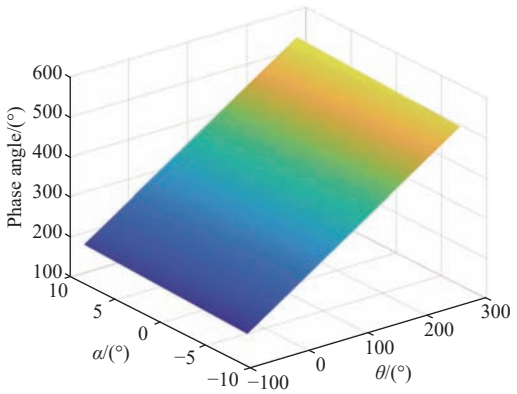

Figure 11 Phase angle response surface of the constraint boundary vector for the case study at different deviation angles (α) of seed and rotational angle of the metering disc (θ)

Table 1 Input parameters for the prediction model in the case study

Parameter	Unit	Value
Coefficient of rolling friction (μ)	Dimensionless	0.06
Gravitational acceleration (g)	m·s^{-2}	9.81
Radius of metering disc (R)	m	0.11
Seed filling correction coefficient (N)	Dimensionless	2.5

The predicted phase angles (ϕ) of the external force vector were plotted as a response surface for each seeder travel speed (Figure 12). The response surfaces showed that the phase angles of the external force vector in the superposition field do not change on

the $\alpha-\phi$ plane, whereas they fluctuate on the $\theta-\phi$ plane. This is true, regardless of the seeder travel speed. It was also observed that the response surface fluctuates more at an increased seeder travel speed.

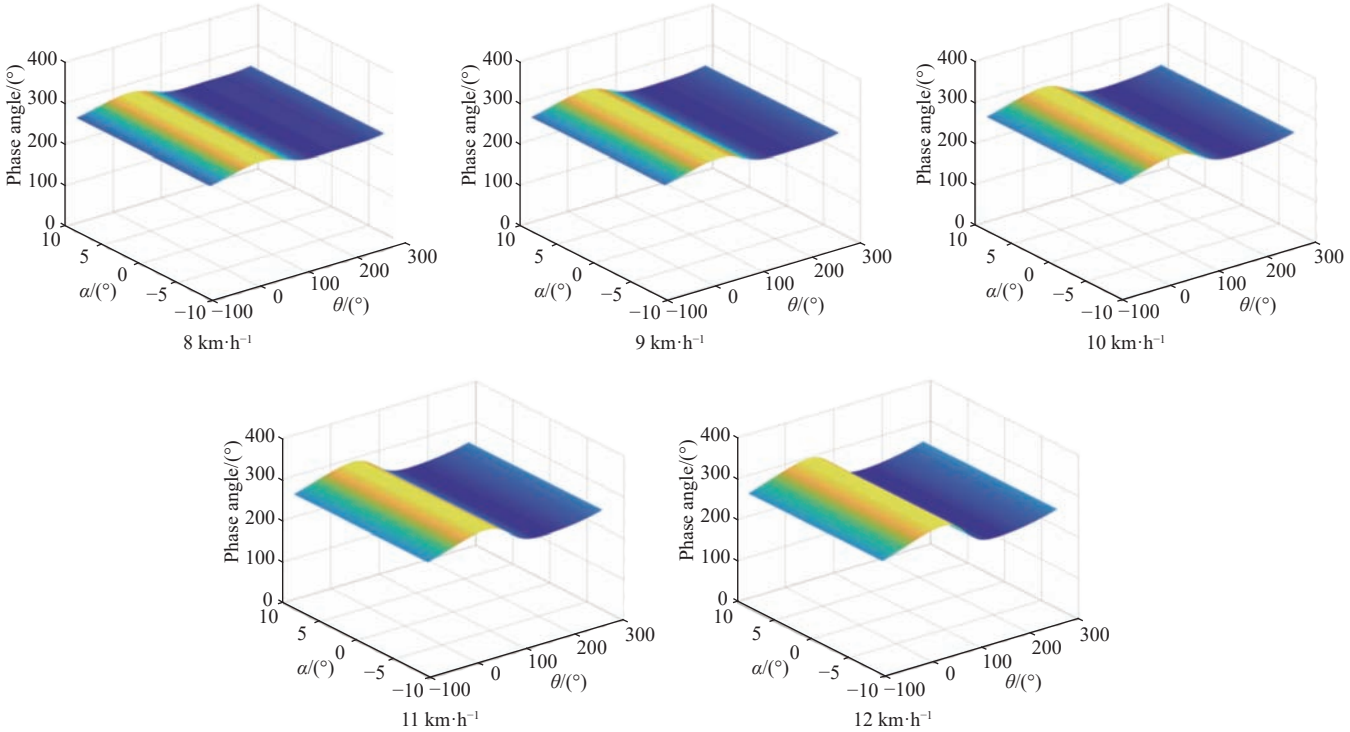

Figure 12 Response surfaces of the phase angle function of the external force vector under different seeder travel speeds for the case study.

3.5 Initial seed clearing angle

When the external force vector coincides with the constraint boundary vector in the superposed field, that marks the beginning of the seed clearing stage. Thus, the theoretical initial seed clearing angle is the interaction of the two surfaces of $(\phi_c(\theta))$ and $(\phi_f(\theta))$, as illustrated by the surfaces at the seeder travel speed of 10 km/h (Figure 13). The phase angle functions were compiled using Python language for different values of α and θ, and the results were then imported into Pycharm software to determine the initial clearing angles of the soybean seeds using the parameters listed in Table 1. The results are discussed in the following section.

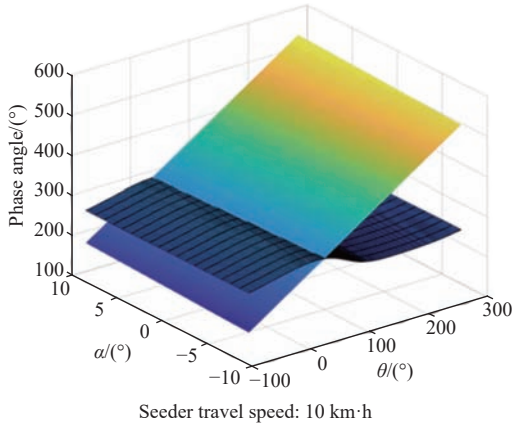

Figure 13 Initial seed clearing angle defined as the interaction of the phase angle functions of constraint boundary vector (the linear surface) and external force vector (the curved surface)

3.6 Model validation results

The seed clearing angles predicted were compared with those measured from the bench tests. Due to the clearing being a very quick process, therefore, researcher was subject to observe model method, the traditional comparative perspective of the interval between 5° to 10°[21,22]. In this study, the high-speed camera was adopted, and the observation accuracy of the test bench was higher than in traditional research. But the measurement of the initial seed clearing angle was still difficult. The observation interval was divided as 3° because of the error that exists in the test experiment. Two sets of results were compared at multiple intervals (18 intervals) so as to observe the distributions of the results[23]. Also, at each interval, the comparison was made for each of five seeder travel speeds (Table 2). With the increase of seeder travel speed, the initial seed clearing angle increased in both the model and bench test. The main reason is that when the working speed increases, the metering disc rotates faster, and thus, the response surface of the phase angle function moves up as shown in Figure 13. As a result, the intersection line of the two response surfaces would move up as well, which leads to greater initial seed clearing angles.

The results of model prediction and bench tests were imported into SPSS17.0 (IBM Company, the US) software for further analyses. The probability distribution of the initial seed clearing angles followed a normal distribution, regardless of the seeder travel speed (Figure 14). Both the model and test values conform to the central limit theorem at all seeder travel speeds. The distribution curves of the bench test are flatter than those of the model predictions, meaning that each of the curves spans over a wider range of the initial seed clearing angle. The central value of the distribution for the model predictions slightly increased with the seeder travel speed (Figure 14a), whereas that of the bench tests slightly decreased (Figure 14b).

Table 2 and Figure 14 showed some discrepancies between the model and test values at a given seeder travel speed. The reason could be due to the various sizes and shapes of the soybean seeds, resulting in variations of the external forces of the seed. That contributed to the discrepancies in the initial seed clearing angles.

Table 2 Model predictions and bench test results of initial seed clearing angles under different seeder travel speeds

Interval/(°)	Seeder travel speed/km·h^{-1}									
	8		9		10		11		12	
	Model	Test	Model	Test	Model	Test	Model	Test	Model	Test
[8,11]	0	0	0	0	0	0	0	0	0	0
(11,14]	0	2	0	2	0	0	0	0	0	0
(14,17]	2	8	0	4	0	0	0	0	0	0
(17,20]	35	32	0	12	0	4	0	0	0	0
(20,23]	71	41	24	20	0	7	0	1	0	0
(23,26]	67	49	57	31	4	17	0	5	0	0
(26,29]	20	32	76	34	49	17	0	9	0	1
(29,32]	5	30	36	43	74	53	15	30	0	3
(32,35]	0	6	7	22	60	53	48	39	0	4
(35,38]	0	0	0	24	12	30	85	50	16	16
(38,41]	0	0	0	5	1	15	44	37	52	27
(41,44]	0	0	0	3	0	3	8	19	84	42
(44,47]	0	0	0	0	0	1	0	4	41	44
(47,50]	0	0	0	0	0	0	0	4	7	33
(50,53]	0	0	0	0	0	0	0	2	0	17
(53,56]	0	0	0	0	0	0	0	0	0	11
(56,59]	0	0	0	0	0	0	0	0	0	2

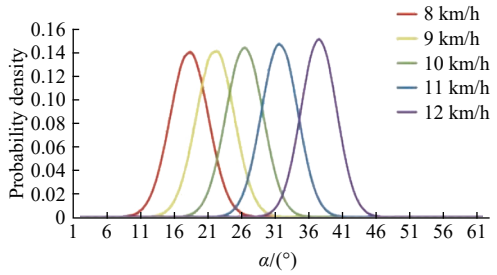

a. Model predictions

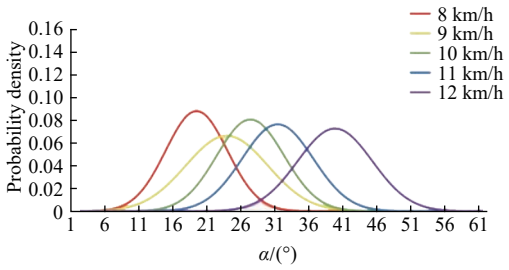

b. Bench tests

Figure 14 Probability distribution of initial seed clearing angle (α) at different working speeds

The agreement between the model predictions and bench test results was further assessed at each of five seeder travel speeds. Over the seeder speed range of 8-12 km/h, the RMSE were from 2.73 to 3.14, and the r between predict and observer were all higher than 0.98 (Table 3). These values are quite low, meaning that the model values were comparable with the test values. This proved that the model had reasonably good accuracy.

Table 3 Relative mean errors (RE) between the model and bench test values

Seeder travel speed/km·h^{-1}	Relative mean errors/%
8	5.23
9	6.49
10	3.08
11	0.61
12	5.37

4 Conclusions

In this study, a prediction model was developed to predict the initial seed clearing angle which is a critical parameter for seed singulation in precision metering process. The model was applied to the existing double-holding seed meter and soybean seeds. The following conclusions were drawn:

The model was capable of dealing with seeds having variable dimensions under variable seeder travel speeds. The approach of using vector fields in complex plane is effective to address the dynamic changes in seed movements and external forces as the seed metering disc rotates.

The direction of the external force vector fluctuates, while the direction of the constraint boundary vector increases, as the rotational angle of the metering disc increases.

The initial seed clearing angle of soybean metered with the double-holding precision meter varied from 11° to 59°, depending on the seeder travel speed.

The model results of the initial seed clearing angle agreed well with the bench test results. The model was validated using only one type of seed and precision seed meter. Caution should be taken when using the model for other types of seed and seed metering device.

Acknowledgements

This work was supported by the National Natural Science Foundation of China (Grant No. 32372009), the National Natural Science Foundation of China (Grant No. 31971802).

[References]

[1] Correia T P D S, Sousa S F G D, Silva P R A, Dias P P, Gomes, A R A. Sowing performance by a metering mechanism of continuous flow in different slope conditions. Engenharia Agrícola, 2016; 36(5): 839–845.

[2] Cay A, Kocabiyik H, May S. Development of an electro-mechanic control system for seed-metering unit of single seed corn planters part I: design and laboratory simulation. Computers & Electronics in Agriculture, 2018; 144: 71–79.

[3] He J, Zhang Z Q, Li H W, Wang Q J. Development of small/medium size no-till and minimum-till seeders in Asia: A review. Int J Agric & Biol Eng, 2014; 7(4): 1–12.

[4] Wang J W, Tang H, Guan R, Li X, Bai H C, Tian L Q. Optimization design and experiment on clamping static and dynamic finger-spoon maize precision seed metering device. Transactions of the CSAM, 2017; 48(12): 48–57. (in Chinese)

[5] Jia H L, Chen Y L, Zhao J L, Guo M Z, Huang D Y, Zhuang J. Design and key parameter optimization of an agitated soybean seed metering device with horizontal seed filling. Int J Agric & Biol Eng, 2018; 11(2): 76–87.

[6] Yu Y, Hu Y R, Shang S Q, Diao L S, Ge R C, Zhang X. Design of motor-driven precision seed-metering device with improved fuzzy PID controller for small peanut planters. Int J Agric & Biol Eng, 2023; 16(1): 136–144.

[7] Nikolay Z, Nikolay K, Gao X J, Li Q W, Mi G P, Huang Y X. Design and testing of novel seed miss prevention system for single seed precision metering devices. Computers & Electronics in Agriculture, 2022; 198: 107048.

[8] Xu J, Sun S L, He Z K, Wang X M, Zeng Z H, Li J, Wu W B. Design and optimisation of seed-metering plate of air-suction vegetable seed-metering device based on DEM-CFD. Biosystems Engineering, 2023; 230: 277–300.

[9] Gao X J, Xie G F, Li J, Shi G S, Lai Q H, Huang Y X. Design and validation of a centrifugal variable-diameter pneumatic high-speed precision seed-metering device for maize. Biosystems Engineering, 2023; 227: 161–181.

[10] Zhao Y X, Jian X D. Analysis of cleaning process of mechanical precision seed-metering device. Transactions of the CSAM, 2006; 37(11): 193–194. (in Chinese)

[11] Li C H, Xia J M, He B. Analysis and experiment of seed metering procedure in scoop metering device with declined disc. Transactions of the CSAM, 2004; 35(3): 68–71. (in Chinese)

[12] Xu J, Cai Z S, Gan Y Q, Zhang L L. Optimization study on seed clearing process for declined disc-scooptype soybean seed metering device based on EDEM. Journal of Northeast Agricultural University, 2018; 49(10): 79–88. (in Chinese)
[13] Xue P, Xia X Y, Gao P Y, Ren D, Hao Y J, Zheng Z Q, et al. Double-setting seed-metering device for precision planting of soybean at high speeds. Trans of ASABE, 2019; 62(1): 187–196.
[14] Yazgi A, Degirmencioglu A. Optimisation of the seed spacing uniformity performance of a vacuum-type precision seeder using response surface methodology. Biosystems Engineering, 2007; 97(3): 347–356.
[15] Yu J Q, Shen Y F, Niu X T, Fu H, Ni T H. DEM simulation and analysis of the clearing process in precision metering device with combination inner-cell. Transactions of the CSAE, 2008; 24(5): 105–109. (in Chinese)
[16] Miller E A, Rascon J, Koller A, Porter W M, Taylor R K, Raun W R, et al. Evaluation of corn seed vacuum metering systems. Transactions of the ASABE, 2012, Dallas, Texas, July 29 - August 1.
[17] An X, Wang S, Duan H Y, Yang C, Yu Y C. Test on effect of the operating speed of maize-soybean interplanting seeders on performance of seeder-metering devices. Procedia Engineering, 2017; 174: 353–359.
[18] Hang C G, Gao X J, Yuan M C, Huang Y X, Zhu R X. Discrete element simulations and experiments of soil disturbance as affected by the tine spacing of subsoiler. Biosystems Engineering, 2018; 168: 73–82.
[19] Dun G Q, Mao N, Gao Z Y, Wu X P, Liu W H, Zhou C. Model construction of soybean average diameter and hole parameters of seed-metering wheel based on DEM. Int J Agric & Biol Eng, 2022; 15(1): 101–110.
[20] Zheng B X, Du X H, Xi Y. A new algorithm of outlier mining in time series data. Control and Decision, 2002; 3: 324–327.
[21] Lei X L, Liao Y T, Li Z D, Cao X Y, Li S S, Wei Y P, et al. Design and experiment of seed feeding device in air-assisted centralized metering device for rapeseed and wheat. Transactions of the CSAE, 2015; 31(20): 10–18. (in Chinese)
[22] Mei Z X, Xia J F, Zhang J M, Du J, Yang Q J, Hu M J, et al. Seeding performance of seed metering device with Spiral tube scooping for rice and wheat. Journal of Huazhong Agricultural University, 2020; 39(5): 136–146. (in Chinese)
[23] Ding H J, Song Y H, Hu Z C, Wu J C, Fan X X. Probability density function of day-ahead wind power forecast errors based on power curves of wind farms. Proceedings of the CSEE, 2013; 33(34): 136–144. (in Chinese)